NUCLEAR DATA AND MEASUREMENTS SERIES

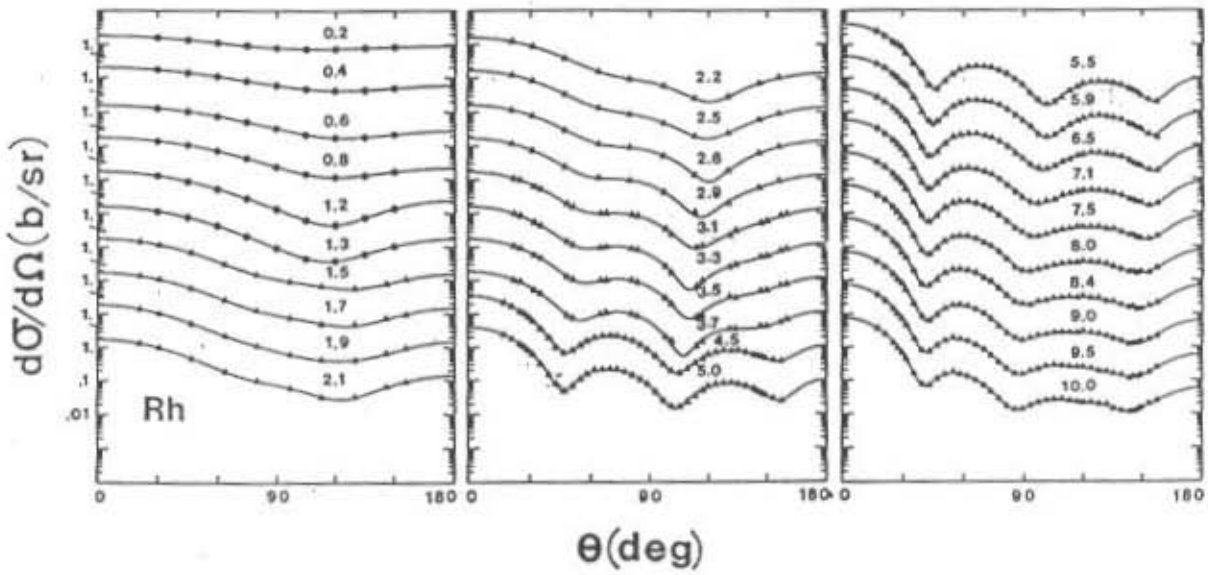
ANL/NDM-151

FAST-NEUTRONS INCIDENT ON HOLMIUM

by

Alan B. Smith

December, 2000



ARGONNE NATIONAL LABORATORY, ARGONNE, ILLINOIS

Operated by THE UNIVERSITY OF CHICAGO

for the U. S. DEPARTMENT OF ENERGY

under Contract W-31-109-Eng-38

Argonne National Laboratory, with facilities in the states of Illinois and Idaho, is owned by the United States Government, and operated by the University of Chicago under provisions of a contract with the Department of Energy.

Disclaimer

This report was prepared as an account of work sponsored by an agency of the United States Government. Neither the United States Government, nor The University of Chicago, nor any agency thereof, nor any of their employees or officers, makes any warranty, expressed or implied, or assumes any legal liability or responsibility for the accuracy, completeness, or usefulness of any information, apparatus, product, or process disclosed, or represents that its use would not infringe privately owned rights. Reference herein to any specific commercial product, process, or service by trade name, trademark, manufacturer, or otherwise, does not necessarily constitute or imply its endorsement, recommendation, or favoring by the United States Government or any agency thereof. The views and opinions of authors expressed herein do not necessarily state or reflect those of the United States Government or any agency thereof, Argonne National Laboratory, or The University of Chicago.

Available electronically at http://www.doe.gov/bridge

Available for a processing fee to U. S. Department of Energy and its contractors, in paper, from:

U. S. Department of Energy
Office of Scientific and Technical Information
P.O. Box 62
Oak Ridge, TN 37831-0062
phone: (865) 576-8401
fax: (865) 576-5728
email: reports@adonis.osti.gov

Nuclear Data and Measurement Series

Reports in the Argonne National Laboratory Nuclear Data and Measurement Series present results of studies in the field of microscopic nuclear data. The primary objective of the series is the dissemination of information in the comprehensive form required for nuclear technology applications. This Series is devoted to: a) measured microscopic nuclear parameters, b) experimental techniques and facilities employed in measurements, c) the analysis, correlation and interpretation of nuclear data, and d) the compilation and evaluation of nuclear data. Contributions to this Series are reviewed to assure technical competence and, unless otherwise stated, the contents can be formally referenced. This Series does not supplant formal journal publication, but it does provide the more extensive information required for technological applications (e.g., tabulated numerical data) in a timely manner.

ANL/NDM-151

FAST-NEUTRONS INCIDENT ON HOLMIUM*

by

Alan B. Smith

Argonne National Laboratory
Argonne, Illinois

December, 2000

Keywords:-
Measured neutron $d\sigma/d\Omega_{el}$ for Ho, 4.5 → 10 MeV. Extensive optical and coupled-channels model interpretations.

---

*This work supported by the United States Department of Energy under contract W-31-109-Eng-38.

PUBLICATIONS IN THE ANL/NDM SERIES

A listing of recent issues in this series is given below. Issues and/or titles prior to ANL/NDM-130 can be obtained from the National Technical Information Service, U. S. Department of Commerce, National Technical Information Service, Technology Administration, Springfield, VA 22161, or by contacting the author of this report at the following address:-

Technology Development Division
Argonne National Laboratory
9700 South Cass Avenue
Argonne, IL 60439
USA

In addition, information on the ANL/NDM Report Series can be found on the Internet at the following URL: http://www.td.anl.gov/reports/ANLNDMReports.html. This Internet address contains complete textual and tabular information.

A. B. SMITH AND P. T. GUENTHER
Fast-Neutron Interaction with the Fission Product ^{103}Rh
ANL/NDM-130, September 1993

A. B. SMITH AND P. T. GUENTHER
Fast-Neutron Scattering from Vibrational Palladium Nuclei
ANL/NDM-131, October 1993

A. B. SMITH
Neutron Interaction with Doubly-Magic ^{40}Ca
ANL/NDM-132, December 1993

A. B. SMITH
Neutron Scattering at Z = 50:- Tin
ANL/NDM-133, September 1994

A. B. SMITH, S. CHIBA AND J. W. MEADOWS
An Evaluated Neutronic File for Elemental Zirconium
ANL/NDM-134, September 1994

A. B. SMITH AND S. CHIBA
Neutron Scattering from Uranium and Thorium
ANL/NDM-135, February 1995

A. B. SMITH
Neutron Scattering and Models:- Iron
ANL/NDM-136, August 1995

A. B. SMITH
Neutron Scattering and Models:- Silver
ANL/NDM-137, July 1996

A. B. SMITH
Neutron Scattering and Models:- Chromium
ANL/NDM-138, June 1996

W. P. POENITZ AND S. E. AUMEIER
The Simultaneous Evaluation of the Standards and Other Cross Sections of Importance for Technology
ANL/NDM-139, September 1997

J. T. DALY and D. L. SMITH

A Compilation of Information on the $^{31}P(p,\gamma)^{32}S$ Reaction and Properties of Excited Levels in ^{32}S

ANL/NDM-140, May 2000

A. B. SMITH

Neutron Scattering and Models:- Titanium

ANL/NDM-141, July 1997

A. B. SMITH

Neutron Scattering and Models:- Molybdenum

ANL/NDM-142, July 1999

R. E. MILLER AND D. L. SMITH

A Compilation of Information on the $^{31}P(p,\gamma)^{33}Cl$ Reaction and Properties of Excited Levels in ^{33}Cl

ANL/NDM-143, July 1997

R. E. MILLER AND D. L. SMITH

A Compilation of Information on the $^{31}P(p,\gamma)^{28}Si$ Reaction and Properties of Excited Levels in ^{28}Si

ANL/NDM-144, November 1977.

R. D. LAWSON AND A. B. SMITH

ABAREX -- A Neutron Spherical Optical-Statistical Model Code:-- A Users Manual

ANL/NDM-145, June 1998.

R. T. KLANN AND W. P. POENITZ

Non-destructive Assay of EBR-II Blanket Elements Using Resonance Transmission Analysis

ANL/NDM-146, August 1998.

A. B. SMITH

ELEMENTAL ABAREX -- A User's Manual

ANL/NDM-147, June 1999.

D. G. NABEREJNEV AND D. L. SMITH

A Method to Construct Covariance Files in ENDF/B Format for Criticality Safety Applications

ANL/NDM-148, June 1999.

A. B. SMITH

Neutrons and Antimony:- Physical Measurements and Interpretations

ANL/NDM-149, July 2000.

A. B. SMITH AND A. FESSLER

Neutrons and Antimony:- Neutronic Evaluations of ^{121}Sb and ^{123}Sb

ANL/NDM-150, July 2000.

Table of Contents

Abstract ---------- 1

1. Introduction ---------- 1

2. Experimental procedures and results ---------- 2

3. Model representations ---------- 3

3-1. Data base ---------- 3
3-2. Spherical optical model (SOM) ---------- 4
3-3. Coupled-channels model (CCM) ---------- 6
3-4. Dispersive coupled-channels model (CCMD) -------- 9

4. Some physical coments ---------- 10

5. Concluding remarks ---------- 14

Acknowledgements ---------- 16

References ---------- 16

A. General ---------- 16
B. Total cross sections ---------- 18
C. Differential-scattering cross sections ---------- 18

ANL/NDM-151

FAST-NEUTRONS INCIDENT ON HOLMIUM

by

Alan B. Smith

Abstract

Differential neutron-scattering cross sections of elemental holmium (i.e., ^{165}Ho) are measured at forty or more scattering angles, at ≈ 0.5 MeV incident-energy intervals, from ≈ 4.5 → 10.0 MeV. These new results are combined with neutron total and scattering cross sections previously reported in the literature to obtain as comprehensive an experimental data base as possible. This data is interpreted in the context of spherical-optical, coupled-channels and dispersive models, with particular attention to the collective excitation of the $K = 7/2^-$ ground-state rotational band of ^{165}Ho. The effect of the collective properties on the model potentials is discussed. Comparisons are made with previous models reported in the literature and with the relevant portions of the ENDF/B-6 evaluated nuclear data file. Generally, the latter evaluation is supported by the present work. Suggestions for future charged-particle and neutron studies of holmium are made.

1. Introduction

Elemental holmium is strongly deformed and mono-isotopic with a complex low-lying excited structure attributed to a number of rotational and vibrational collective bands [NDS]. The first of these is the ground-state $K = 7/2^-$ rotational band with the first two excited states at ≈ 94.7 and 209.8 keV. One would expect a strong coupling between the ground-state and these two excited states. There have been remarkably few measurements of neutron scattering from holmium (e.g. [Mea+71], [Fas+69], [GT63], [Wag+65]), and only one scattering distribution above 10 MeV (11.1 MeV, [FCR77]). Apparently, there are no measurements of ^{165}Ho(p,p) scattering. Holmium becomes ferromagnetic at low temperatures, and studies of polarization effects on the neutron total cross sections of holmium using polarized beams and aligned targets have been reported ([Wag+65], [Tam65], [MRT66]). They demonstrated a small deformation effect on the total cross section. With high spins, odd parity, strong collective effects and complex low-energy excitations including strong compound-nucleus contributions, model interpretations of ^{165}Ho(n,n) processes are tedious even with recently available

calculational tools.

The present experimental work was undertaken to fill some of the void in the knowledge of the ^{165}Ho neutron-scattering processes, and to provide quantitative models for both basic and applied purposes. ^{165}Ho is on the upper edge of the fission-yield mass curve, with small thermal-fission yields. However, as the incident-neutron energy increases the ^{165}Ho fission yields increase and become significant. Thus there is an applied interest in the neutron interaction with holmium from the points view of fast-reactor and fusion-energy systems and for the general understanding of the neutron interaction with highly-collective nuclei in the fission-product region.

2. Experimental procedures and results

The present measurements were made using the fast time-of-flight method long employed at this Laboratory, as described in refs. [CL55] and [Smi+92], and refs. cited therein. The scattering sample was a 2 cm diameter and 2 cm long cylinder of high-purity holmium (99+%) placed ≈ 12 cm from a pulsed D(d,n)^{3}He neutron source at a 0^o reaction angle. The incident-neutron energy spread at the sample varied from ≈ 300 keV at 4.5 MeV to ≈ 100 keV at 10 MeV. The scattered-neutron resolution was ≈ 450 keV, and thus all the "elastic"-scattering results of the present work contained inelastic contaminations from levels up to excitations of ≈ 450 keV. These perturbations were treated in the interpretations as discussed below. All scattering measurements were made relative to the standard H(n,p) cross section [CSL83] and corrected for angular-resolution, multiple-event and beam-attenuation effects using monte-carlo methods [Smi91].

The differential "elastic"-scattering measurements were made at 40 or more angles and at incident-neutron energy intervals of ≈ 0.5 MeV from ≈ 4.5 → 10 MeV, distributed over scattering angles between ≈ 17^o and 160^o. The normalization uncertainties in these measurements were estimated to be ≈ 2 → 3 % and the statistical uncertainties varied from ≈ 2% or less in regions of large cross sections to as much as ≈ 10% at the extreme minima of the distributions at back angles and higher energies. These experimental results and their uncertainties are illustrated in Fig. 2-1. Comparisons with the sparse values previously reported in the literature are discussed in the following sections.

3. Model representations

3-1. Data base

The data base used in the interpretations consisted of the total cross sections, the "elastic"-scattering cross sections and, to a lesser extent, the inelastic-scattering cross sections. The total cross sections were obtained from the National Nuclear Data Center [NNDC] as defined in the total-cross-section portion of the reference list. Some of these data sets involve a large number of numerical values. In those cases the data was energy-averaged over 50 keV intervals below 0.5 MeV, over 100 keV from 0.5 to 5.0 MeV and over 200 keV at higher energies in order to smooth fluctuations and to reduce the number of data points to be handled in the subsequent interpretations. These energy-averaged total-cross sections are illustrated and compared with the ENDF/B-6 [ENDF] values in Fig. 3-1-1. The definition is quite good, although there is a somewhat unusual shape in the low-MeV region that is not consistent with the energy dependence of the common spherical optical model.

The differential "elastic"-scattering data base was constructed from; i) The present experimental results. ii) Early Argonne measurements [Mea+71]. This reference contains a large number of distributions. In order to reduce the number and smooth the data they were averaged over ≈ 200 keV incident-energy intervals. And iii) the literature as defined in the differential-scattering portion of the reference list. It is not a very detailed scattering data base. Furthermore, there are considerable questions as to experimental resolution. All but a few of the lowest-energy distributions contain varying inelastic-scattering contributions from the first few excited levels. Only in the present results is this inelastic-scattering perturbation reasonably understood. Some of the available experimental information has been "corrected" for "compound-nucleus" scattering in an uncertain manner [FCR77], and direct inelastic scattering is increasingly important with energy. There is no elastic-scattering information above ≈ 11 MeV, and only at the lowest energies is the elastic-scattering contribution reasonably resolved from the inelastic-scattering contributions. A few of the scattering distributions reported in the literature were abandoned as being too fragmentary for model interpretations and/or because of large inconsistencies with the body of the information. The final differential-scattering data base is summarized in Fig. 3-1-2.

Experimental inelastic-scattering results were given some consideration. Such information is confined to refs. [Fas+69] and [Mea+71]. Ref. [Fas+69] contains only information resulting from the excitation of many levels in broad bands, generally starting with excitations of ≈ 0.9 MeV. The contributing levels are not well defined or well known. Therefore, the results are not useful for testing models in the present context. Ref. [Mea+71] does give some detailed experimental information

relevant to the excitation of the first two excited states of the $K = 7/2^-$ ground-state rotational band. These are the $9/2^-$ level at 94.7 keV and the $11/2^-$ level at 209.8 keV [NDS]. These values are useful for testing the validity of the direct-reaction calculations. This experimental inelastic-scattering information is illustrated in Fig. 3-1-3. Ref. [Mea+71] also gives some information relevant to the broader resolution of levels at higher-energy excitations, as discussed below.

Throughout the above data base the experimental uncertainties stated by the various authors were accepted. However, it is evident that the authors often had quite different concepts of uncertainties. The above is not an excellent experimental data base, particularly in the context of a strong collective rotor with high spins and a number of unresolved low-lying levels.

3-2. Spherical optical model (SOM)

Elemental holmium (^{165}Ho) is an odd nucleus with a negative-parity, high-spin, ground-state ($7/2^-$). At least 30 levels are known to exist at excitations of $\lesssim$ 1.0 MeV, the spins and parities of which are not all certain [NDS]. These levels are attributed to at least thirteen collective rotational and/or vibrational bands [NDS]. All of the modeling of the present work considered the effects of the first 20 of the discrete levels up to excitations of $\approx$ 0.7 MeV. The corresponding spins and parities were taken from ref. [NDS]. Compound-nucleus contributions from these discrete levels were explicitly calculated using the Hauser-Feshbach statistical formulation ([HF52], [Wol51]), as modified for fluctuation and correlation effects by Moldauer [Mol80]. The latter corrections were usually small due to the high spins and the large number of levels. The compound-nucleus contributions due to these discrete levels were combined in the calculations in a manner that was estimated to be consistent with the experimental resolutions of the particular measurements. As noted above, these estimates are uncertain in some of the cases. Compound-nucleus contributions from levels above $\approx$ 0.7 MeV were treated in a statistical manner using the theory and parameters of Gilbert and Cameron [GC65].

Throughout this work the real-potential was assumed to have the Woods-Saxon form. The surface-imaginary-potential was assumed to have the derivative-Woods-Saxon form. When a volume-imaginary-potential was considered it was taken to have the same Woods-Saxon shape and geometric parameters as the real potential [Hod94]. A real spin-orbit potential of the Thomas form was used. For the spherical calculations the spin-orbit parameters were fixed to those of ref. [WG86], and for the coupled-channels calculations to those of ref. [You86]. These alternate spin-orbit choices gave essentially the same results,

in the context of the present work. No spin-spin potential was considered as detailed investigations of polarization effects in holmium indicate that it is very small [FHM69].

The SOM was derived by chi-square fitting the above data base in two sequential steps, using the spherical optical-model code ABAREX [Mol82]. The first step determined the the potential geometric parameters by fitting each of the differential scattering distributions of the data base illustrated in Fig. 3-1-2. Initially, six-parameter fits (real- and imaginary-potential strengths, radii and diffusenesses) assuming only surface absorption were made. From these the average value of the real diffuseness (a_v) was determined. a_v was then fixed to that average value and five-parameter fits made from which the average real-potential radius (r_v) was determined. Throughout this work the "reduced radius" is used where the full radius $R_i \equiv r_i \cdot A^{1/3}$ and A is the target mass. The selection of r_v is somewhat uncertain as the various values resulting from the fitting scattered due to the well-known Vr^2 ambiguity in the context of a less than comprehensive and precise data base. With a_v and r_v fixed, four parameter fits were used to determine the imaginary-potential radius (r_w), followed by three parameter fits from which the imaginary-potential diffuseness (a_w) was fixed. The scatter in the a_w values was rather large, in part due to the Wa_w ambiguity. The variation of these geometric parameters in the fitting of the data base did not suggest an energy dependence, therefore the SOM geometric parameters were assumed to be energy independent.

The second sequential step in the determination of the SOM parameters took advantage of the feature of ABAREX that makes possible the concurrent fitting of differential and total cross sections over a wide energy range. In doing so, it was assumed that the SOM geometric parameters were constant with energy and fixed to the values determined in the above first fitting sequence. It was further assumed that the real- and imaginary-potential strengths had a linear energy dependence. That is a reasonable physical assumption as one would expect the real-potential strength to decrease with energy due to the effect of the non-locality of the nuclear force in a finite nucleus [PB62], and, conversely, that the imaginary strength would increase with energy up to approximately 20 MeV to account for the opening of more channels. In this second fitting sequence the experimental data base consisted of the differential "elastic" scattering distributions shown in Fig. 3-1-2 and total cross sections taken from the data base of Fig. 3-1-1. This composite data base, extending from 0.05 → 20 MeV, was then chi-square fitted as a single entity using the capabilities of ABAREX. Little of the differential experimental data fully

resolves the elastic-scattering from inelastic-scattering components. Therefore most of the calculations again combined elastic- and inelastic-differential distributions to approximate the experimental resolutions to the extent they were discernible. When dealing with both differential and total cross sections in the fitting procedure, attention must be given to the weighting of the two types of information. The measurements are quite different, with a different character of the uncertainties. If attention is not given to the weighting, one or the other type of information will dominate the results. In the present comprehensive fitting a number of alternate weightings were examined, in addition to the experimental uncertainties cited by the respective authors. Experience indicated that, for this particular data base, the best results were obtained by weighting the total-cross-section values by a factor of twenty more than the individual differential-scattering values. Finally, four parameter fits using the combined differential and total cross-sections were carried out to fix the real- and imaginary-potential strengths and their linear energy dependencies. The final resulting SOM model parameters are given in Table 3-2-1. In this Table, and in all potential-parameter tables in this work, the parameters are given to precisions that make it possible to accurately reproduce the calculated results. These precisions do not necessarily imply uncertainties.

The SOM parameters of Table 3-2-1 gave a remarkably good description of the experimental total cross sections from a few keV to 20 MeV and above, as illustrated in Fig. 3-2-1. However, they lead to a S_o strength function ≈ 1.5 times as large as deduced from measurements and a S_1 strength function ≈ 3.5 times as large as the experimental values [MDH81]. The SOM description of the differential-scattering data is only qualitative at best. This is not surprising as most of the measured distributions contain large contributions from the direct inelastic excitation of the low-lying levels that are simply inconsistent with the SOM assumption of compound-nucleus inelastic scattering alone. This matter is further discussed below.

3-3. Coupled-channels model (CCM)

Elemental holmium (^{165}Ho) is clearly a highly collective nucleus [NDS]. Extensive coulomb-excitation, radioactive-decay and particle-reaction studies indicate a wealth of collective structures which can be generally described in the context of the unified collective model of Mottelson and Nilsson ([MN59]. The first of these is the single-particle ground-state rotational band $7/2^-\{K=7/2, [523], (3/2^2, 7/2^1)\}$, as given in ref. [NDS]. The next single-particle rotational band should be based on the $1/2^+\{K=1/2, [411], (3/2^2, 1/2^1)\}$ configuration and the first level of it is associated with the reported 429 keV level [NDS].

The next single-particle rotational band is a $7/2^+[404]$ configuration and its first level is associated with the reported 715 keV level. Pairing effects can influence the structure of collective nuclei [Pre62]. The reported ^{165}Ho band sequence starting with the 361 keV level has been attributed to the pairing of 7/2 particles leading to a single particle configuration of $3/2^+\{K=3/2, [411], (3/2^1, 7/2^2)\}$ [BSC64]. In addition, a number of the low-lying excitations of ^{165}Ho are attributed to at least three γ-vibrational bands and to several more particle-based bands [NDS]. In total, thirteen collective bands are cited in ref. [NDS] as contributing to holmium structure at excitations below ≈ 1.5 MeV. The energies of the levels within a given band can be estimated from the familiar expression [Pre62]

$$E_J = \frac{\hbar^2}{2I}\{J(J+1) + \delta_{K,1/2}a(-1)^{J+1/2}(J+1/2)\}. \qquad (3\text{-}3\text{-}1)$$

This complexity of the low-energy holmium excited structure is far beyond the resolution of relevant inelastic-neutron scattering measurements. Therefore, the present interpretation of the collective aspects of the neutron interaction with ^{165}Ho was confined to the three yrast levels of the $7/2^-$ ground-state rotational band. This simplified calculational model then couples these first three levels ($7/2^-$ ground state, $9/2^-$ 94.7 keV first-excited level, and $11/2^-$ 209.8 keV second excited level) of this ground-state rotational band assuming β_2 and β_4 deformation parameters for the simple rotor. Initially, it was assumed that $\beta_2 = 0.3$ and $\beta_4 = -0.02$. This β_2 value is consistent with the results of coulomb-excitation studies ([OE60], [FHM69]), and other considerations of the neutron interaction with ^{165}Ho ([You86], [Wag+65], [FH62], [AFM65]), while the β_4 follows systematics in this mass region. The effects of considering alternate choices of β_2 and β_4 are considered below. With these assumptions a comprehensive coupled-channels model-fitting procedure was carried out, including the compound-nucleus effects discussed in Section 3.2, above. All of the CCM calculations employed the coupled-channels method [Tam65], implemented with the computer code ECIS96 [Ray96]. The geometric parameters were determined from the differential distributions in the same manner as described above for the SOM. They were very close to the parameters of ref. [You86] which have been used over a wider energy scope. Therefore, the geometries of ref. [You86] were adopted for the subsequent 2-parameter fitting determining potential strengths. The resulting final set of CCM parameters is given in Table 3-3-1. They give a very good description of the total

cross sections to at least 20 MeV, as illustrated in Fig. 3-3-1. The differences between calculated and measured values are generally well within the experimental uncertainties alone. The differential "elastic" scattering experimental results are also reasonably described as shown in Fig. 3-1-2. At low energies, where the reported measurements are said to resolve the elastic scattering from inelastic scattering, the agreement between calculation and measurement is reasonably good, despite the fact that the measurements are approximately thirty years old. For incident energies of $\approx$ 1.0 $\rightarrow$ 1.5 MeV the resolution of the measurements is not clear. Therefore, Fig. 3-1-2 shows several calculated curves for each of these questionable energies, corresponding to calculated elastic, elastic + first inelastic and elastic + first and second inelastic groups. It appears that the 0.93 MeV distribution is essentially due to elastic scattering, while the 1.2 MeV distribution includes the elastic and first inelastic groups. There are uncertainties associated with 1.41 MeV group that are not resolved. The distributions from $\approx$ 4.5 $\rightarrow$ 10 Mev come from the present measurements and their resolution functions are reasonably known. On the whole the agreement between measured and calculated differential distributions in this region is quite good with only some relatively minor discrepancies near 120 deg. at $\approx$ 7 $\rightarrow$ 8 MeV. The agreement for the 11 MeV distribution [FCR77] is also reasonably good except at very back angles. As noted elsewhere herein, the reported experimental 11 MeV distribution has been "corrected" for compound-nucleus contributions. Those corrections are not well specified and, certainly, the inelastic contamination of the measurements at this energy is primarily due to direct-reaction processes. Whether or not these were considered in the "corrections" is not known to the author. Therefore, at 11 MeV, Fig. 3-1-2 shows comparisons with the calculated elastic scattering, elastic + first inelastic scattering and elastic + first and second inelastic scattering groups. The results suggest that the corrected measurements most closely approach the elastic + first inelastic distributions. The CCM potential leads to strength functions that are in qualitative agreement with those deduced from experiment [MDH81], the calculated S_o is $\approx$ 30% larger than the experimental value and S_1 value $\approx$ 20% larger.

While the measured discrete inelastic-scattering excitation of the ground-state rotational band is approximately thirty years old [Mea+71] it does give some support to the CCM model. As illustrated in Fig. 3-1-3, the CCM reasonably describes the excitation of the two yrast excited states of this band. The model somewhat under-predicts the excitation of the 94.8 keV level at lower energies. This may be a consequence of an under-prediction of the compound-nucleus (CN) contribution due to competition from the continuum inelastic scattering. At higher energies where the excitation cross section of this level is primarily due to direct inelastic scattering (e.g., $\geq$ 1.0 MeV) the agreement between measurement and calculation is quite good.

The cross sections for the inelastic excitation of the 209.8 level of the ground-state rotational band are very well described by the CCM (see Fig. 3-1-3). In the excitation of both the first two excited levels of this band, it is clear that the direct reactions of the CCM are a primary contribution as the energy increases.

The inelastic-scattering calculations can be extended to higher excitations using compound-nucleus contributions and compared with the measured results of ref. [Mea+71]. Such comparisons are difficult as the experimental values consist of complex composites of discrete-scattering contributions. Just what reported levels contribute to which observed inelastic excitation is not always clear. However, given all these uncertainties, the comparisons are encouraging, as illustrated in Fig. 3-3-2. All the calculated results above the excitation of the first two levels, shown in this figure, are due entirely to CN contributions.

3-4. Dispersive coupled-channels model (CCMD)

It is well known that there is a dispersion relationship linking real and imaginary potentials and reflecting causality ([Sat83], [Lip66], [Pas67], [Fes58]). This relationship can be expressed in the form

$$J(E)_v = J(E)_{HF} + \frac{P}{\pi} \int_{-\infty}^{+\infty} \frac{J_w(E')}{E - E'} dE', \qquad (3\text{-}4\text{-}1)$$

where J_{HF} is the local-equivalent Hartree-Fock potential, J_w is the strength of the imaginary potential (in volume-integral-per nucleon) and "P" denotes the principle value of the integral. This integral can be broken into surface, ΔJ_s, and volume, ΔJ_{vo}, components

$$\Delta J_s = \frac{P}{\pi} \int_{-\infty}^{+\infty} \frac{J_s(E')}{E - E'} dE' \qquad (3\text{-}4\text{-}2)$$

and

$$\Delta J_{vo} = \frac{P}{\pi} \int_{-\infty}^{+\infty} \frac{J_{vo}(E')}{E - E'} dE'. \qquad (3\text{-}4\text{-}3)$$

Then $J_v(E) = J_{eff}(E) + \Delta J_s(E)$ and $J_{eff}(E) = J_{HF}(E) + \Delta J_{vo}(E)$, where $J_s(E)$ and $J_{vo}(E)$ are surface and volume imaginary-potential strengths, respectively. J_{HF} and ΔJ_{vo} are approximately linear functions of energy in the energy range of the present considerations. Combined, they determine J_{eff} but the two components can not be experimentally distinguished. In the

present work J_{HF} approaches J_{eff} as ΔJ_{vo} is small below 20 MeV. Thus, the effect of Eq. 3-4-1 is to add a surface component to the real Woods-Saxon potential consisting of some fraction of J_s. The magnitude of this contribution was evaluated from the CCM potential (Table 3-3-1) using the methods of Lawson et al. [LGS87]. In doing so it was assumed that the imaginary potential was entirely a surface effect up to 25 MeV and then this surface component fell linearly to zero at 60 MeV. Concurrently J_{vo} was assumed to linearly increase from zero at 25 MeV to 60 MeV where it took the J_s 25 MeV value and then remained energy independent on to higher energies. The imaginary potential was assumed zero at the Fermi Energy (E_F) and to have a quadratic energy dependence to zero energy. In addition, the entire imaginary potential was taken to be symmetric about E_F [JLM77]. The E_F was taken to be -7.116 MeV as determined from the mass tables [Tul90]. With these assumptions, the calculated fraction of the surface imaginary potential to be added to the real potential was essentially a linear function of the energy, falling from approximately unity at zero energy to ≈ 0.1 at 20 MeV.

With the addition of the above surface dispersion contribution to the Woods-Saxon real potential the fitting procedure of the CCM was repeated. The potential geometries were taken to be the same as for the CCM except for the real radius, r_v. The chi-square fitting to each of the differential distributions determined the real- and imaginary-potential strengths and the real radius. The latter should differ from that of the CCM as a surface component has been added to the real potential. The resulting CCMD potential parameters are given in Table 3-4-1. They lead to total cross sections very similar to those obtained with CCM and shown in Fig. 3-3-1. The differences between the two calculations and the experimental values are generally less than the experimental uncertainties alone. The differential scattering calculated with the CCMD is compared with the measured values in Fig. 3-4-1. The comparisons are nearly identical to those obtained with the CCM and shown in Fig. 3-1-2. A careful study of the two figures may suggest that the results obtained with the CCMD are very slightly preferable. Inelastic excitation of the first two members of the ground-state rotational band as calculated with the CCMD is nearly identical to that obtained with the CCM and illustrated in Fig. 3-1-3.

4. Some physical comments

The SOM gives a good description of the observed total cross sections. It can not describe the observed differential scattering as the large collective component is not inherent in the model. However, the simple SOM may be useful for such things as neutron capture calculations or as a starting point for DWBA

calculations. The SOM parameters setforth in Table 3-2-1 are unusual and physically unattractive. The real potential radius is significantly (≈ 3%) less than predicted by systematics ([Smi+97A], [Chi+90]). The real-potential diffuseness (a_v) is unusually small. The real-potential strength falls with energy, but only very slowly, at a rate less than one would expect from non-locality effects alone [PB62], and is generally ≈ 15% smaller than indicated by SOM systematics ([Smi97A], [Chi+90]). The imaginary potential decreases with energy, contrary to what one would expect as more channels open with increasing energy. The imaginary radius is reasonable but the imaginary diffuseness is unusually large. Thus the present SOM may be a viable tool for some pragmatic purposes, but it is not particularly attractive from the point of view of physical understanding. The unusual SOM parameters probably reflect the application of a SOM to a highly collective target. Other SOM's for holmium found in the literature have some of the same shortcomings.

The CCM parameters (Table 3-3-1) are very similar to those of ref. [You86], explicitly so for real- and imaginary-potential geometries. The energy dependence of the real potential is somewhat larger than that of ref. [You86], and the surface absorption is less in the present case. However, the present CCM does not include a volume absorption as does the potential of ref. [You86], as discussed below.

The CCMD parameters are a reasonable extension of the CCM model. The real-potential strength (J_v) is somewhat smaller than that of the CCM, as one would expect as it does not include the dispersive surface contribution to the real potential. Indeed, the difference is approximately the ΔJ_s of Eq. 3-4-3, as it should be. The r_v of the CCMD is somewhat smaller than that of the CCM, as it too should be, since a surface real potential has been added to the potential. In other words, the CCM and CCMD models are quite consistent, and both give good descriptions of the data base.

The present interpretations assumed β_2 and β_4 deformations as described in Section 3-3. Alternate choices were investigated extending from $\beta_2 = 0.2 \rightarrow 0.4$ and $\beta_4 = -0.02$ or 0.0. Repeating the CCM fitting, with consequent adjustment of model parameters, no particular improvement in the total-cross section description was realized. Concurrently, there was no notable improvement in the description of the differential-scattering distributions. Various choices of β_2 did not generally improve the description of the inelastic excitation of the ground-state rotational band shown in Fig. 3-1-3. The differences between calculation and measurement illustrated in that figure (primarily for the 94.8 keV level) are largely due to compound-nucleus effects. The experimental data does not appear sufficient to better define the

β_2 and β_4 values. It was noted that the differential distributions are very sensitive to the choices of β_2 and β_4 at large scattering angles, e.g. at $\approx 175 \rightarrow 180$ deg. Neutron measurements in that angular range are difficult and require special techniques. As a result they are very seldom made, and there is no such information available for ^{165}Ho. Interestingly, The same large-angle scattering information is, unlike the common angular distributions, sensitive to the neutron polarization [Smi80]. Theoretical considerations, such as the core-polarization model [MBA75], can give guidance as to deformations applicable to neutron, proton and electro-magnetic effects, particularly for nuclei near shell closures. Holmium is not near a shell closure, and essentially nothing is experimentally known about proton interactions with holmium.

It is well known ([Lan62], [GS58]) that proton and neutron potential strengths are related through the expression

$$J_i = J_i^o(1 \pm \xi_i \cdot \eta) \qquad (4\text{-}1)$$

where J_i are potential strengths expressed as volume integrals per nucleon, η is the asymmetry (N - Z)/A, "i" may be v or w for real or imaginary potentials and ξ_i is a constant equal to ≈ 0.5 for the real potential and to ≈ 1.5 for the imaginary potential [Smi97]. The "+" is used for protons and the "-" for neutrons. The present CCM results lead to a $J_v^o = 490.4 - 3.927 \cdot E$ for holmium. This expression is $\approx 5\%$ larger at zero energy than values reported from the interaction of neutrons and protons with similarly deformed molybdenum nuclei [Smi97], but the difference decreases with energy and at 20 MeV the holmium and molybdenum results are essentially identical. The relationship of Eq. 4-1 is very useful in constructing unified neutron and proton nuclear potentials. However, for that approach to be effective one must have good proton potentials. Unfortunately, the experimental data for developing them is generally lost in the mists of time. In the particular case of holmium, the author could find no proton scattering or associated potentials of any kind in the literature. The information specialists at the NNDC reached a similar conclusion, and there are no holmium proton potentials listed in the compilation of ref. [PP76]. It is unfortunate, and particularly so in the present context, that (p,p) scattering studies have been so sparse and poorly documented. A wealth of information is either not available or lost.

It is generally believed that, as the energy of the incident particle increases the absorption term of the potential slowly changes from a surface to a volume effect ([Hod71], [BG69]). The energy of such a transition is of some debate. For example, in the case of ^{165}Ho the model of ref. [You86] introduces a

volume-absorption term in the potential at 8.3 MeV, and it increases with energy. A volume-absorption Woods-Saxon term was introduced in both SOM and CCM models and the above-described fitting repeated. These endeavors did not yield any clear evidence that volume absorption was a factor at the energies of the present work. That conclusion might change with a better data base, and almost certainly would change if one goes to much-higher energies. It should be clearly understood that all of the present model considerations are strictly applicable only to energies of less than 20 MeV.

The present CCM potential implies an effective mass, m^*, that can be compared with the values implied by the non-locality of the nuclear force as discussed, for example, in refs. [BLM54], [Bru+56], [PB62], [Bet56] and [WWG60]. These concepts have been further studied by Brown et al. ([BGG63], [BDS79]) using a dynamic theory of vibrations. It is shown in refs. [BDS79], [MN81] and [Bau+82] that the nonlocality leads to the expression

$$\frac{m^*}{m} = 0.64 + 0.36[1.0 + |E - E_F|/(2\hbar\omega_o)]^{-2} \qquad (4\text{-}2)$$

where "m" is the nucleon mass, "m^*" the effective nucleon mass, E the energy in MeV, and $\hbar\omega_o = 41/A^{1/3}$. Concurrently,

$$\frac{m^*}{m} = 1 - \frac{dV_L}{dE}, \qquad (4\text{-}3)$$

where V_L is the local real potential. Well away from E_F Eq. 4-2 leads to $\frac{m^*}{m}$ values of $\approx$ 0.68 which is reasonably consistent with nuclear matter estimates [GPT68]. The CCM and Eq. 4-3 clearly lead to $\frac{m^*}{m}$ ratios of $\approx$ 0.63. This is slightly smaller than one would perhaps like, and may suggest that the linear energy dependence of the CCM real potential is slightly too large. At the same time the zero end point of the CCM is $\approx$ 125 MeV which is smaller than estimated from global analysis [Bau+82], again suggesting a too strong energy dependence of the CCM real potential. The situation is not improved with the CCMD model as sometimes found in other studies [Smi97A].

The present CCM potential bears a strong similarity to the coupled-channel potential of Young [You86]. Indeed the geometries are explicitly identical. The only major difference is the omission of volume absorption in the present work. As noted above, it doubtlessly would be necessary at higher energies. At the lower energies of the present work the the potential of ref. [You86] agrees very well with the CCM. The

only notable difference is a slightly weaker energy dependence of the real potential than following from the present work. In some contexts that may be an advantage (see Eq. 4-3). The potential of [You86] was the basis of the ENDF/B-6 evaluation described below and the comparisons given there illustrate the close agreement of the results obtained with the two models. A CCM potential was developed from some holmium neutron-scattering and total cross section measurements in ref. [Fas+69]. It is not as well defined as that of the present work or that of ref. [You86], but it is qualitatively consistent with both.

The present work can be used to test major portions of the ENDF/B-6 (MAT-6725) holmium evaluated file [YA88]. That file was assembled without the benefit of the new experimental information presented herein, and without the recently available calculational tools [Ray96]. Despite these facts, the major portions of the file that can be tested with the present work appear to be very good. For example, in Fig. 4-1 evaluated total and elastic-scattering cross sections as given by ENDF/B-6 and the present CCM model are compared. The agreement is excellent from a few keV to 20 MeV. Any very minor differences are well within the uncertainties in the underlying experimental measurements alone. This agreement extends to the differential elastic-scattering distributions, as illustrated in Fig. 4-2. Certainly, there are few, if any, applications that would be sensitive to the very small differences in elastic scattering illustrated in Fig. 4-2. Comparisons of inelastic scattering are not quite as good as illustrated in Fig. 4-3, but the differences would probably have little effect on the large majority of applications. Fig. 4-3 suggests that the present CCM model leads to somewhat larger compound-nucleus contributions to discrete inelastic scattering in the few-MeV region than incorporated in the ENDF/B-6 evaluation, and even the present CN contribution to to the excitation of the first-excited level may be too small at low energies. As is clear from the above discussion, there is no experimental evidence to resolve this question and it will be extremely difficult to do so given the complex excited structure of ^{165}Ho. All in all, the present work very much supports the ENDF/B-6 evaluation.

5. Concluding remarks

The experimental aspects of this work provided detailed knowledge of "elastic" neutron scattering from elemental holmium from $\approx$ 4 $\rightarrow$ 10 MeV, a region where there was very little prior experimental information. This new work, together with some old low-energy measurements at this laboratory forms the body of the knowledge of the fast-neutron scattering from holmium. There is only a handful of other experimental results. The data base constructed from the available experimental information was used to develop spherical-optical (SOM), coupled-channels (CCM) and dispersive-coupled-channels (CCMD) models. These models are

strictly applicable only up to 20 MeV. The spherical-optical model gave a good representation of the total cross sections but failed to appropriately describe the partial cross sections of the strongly deformed ^{165}Ho. The CCM, giving consideration to the K = 7/2- ground-state rotational band, was far more successful in describing the various facets of the neutron interaction and is a good tool for future basic and applied calculations. Consideration of dispersive effects lead to the CCMD dispersive coupled-channels model. It described the neutron interaction with holmium to approximately the same accuracy as the simpler coupled-channels model. There was no strong advantage to the added complexity of the dispersive interpretation. These measurements and interpretations provide useful tools for future basic and/or applied work. The results also very much support the ENDF/B-6 evaluation of holmium.

Even with the present work, the knowledge of the neutron and proton interaction with ^{165}Ho remains remarkably poor. Before there can be substantive improvement in the knowledge and interpretation of the neutron interaction it is essential that:-

i) There be some careful ^{165}Ho (p,p) experimental studies from the coulomb barrier to at least 30 MeV. There appears to presently be no information of this type.

ii) High-resolution neutron scattering measurements should be made up to incident neutron energies of several MeV. What results are available are approximately 30 years old and do not significantly extend above ≈ 1.0 MeV. Contemporary experimental techniques should considerably improve the understanding of the discrete inelastic-scattering process.

iii) Experimental understanding of total cross sections of ^{165}Ho is reasonably good up to ≈ 15 MeV. At higher energies the knowledge becomes fragmentary. Total neutron cross sections should be measured with care across a wide energy range stretching up to at least 50 MeV.

iv) There should be a few measured scattered-neutron angular distributions at incident energies from ≈ 12 → 30 MeV with well specified scattered-neutron resolutions. At present there is no information of this type. It is a common problem in fast-neutron physics.

Acknowledgements

The author gratefully acknowledges the data support of the National Nuclear Data Center, the guidance of Dr. J. Raynal in the use of the computational code ECIS, and the many helpful remarks of Dr. P. Young.

References

A. General

[AFM65] Ambler E., Fuller E. and Marshak H., Phys. Rev. 138 B117 (1965).

[Bau+82] Bauer M., Hernandes-Saldana E., Hodgson P. E. and Quintanille J., J. Phys. G8 525 (1982).

[BDS79] Brown G., Dehesa J., and Speth J., Nucl. Phys. A330 290 (1979).

[Bet56] Bethe H., Phys. Rev. 103 1353 (1956),

[BG69] Becchetti F. and Greenlees G., Phys. Rev. 182 1190 (1969).

[BGG63] Brown G., Gunn J., and Gould P., Nucl. Phys. 46 598 (1963).

[BLM54] Brueckner K., Levinson C. and Mahmound H., Phys. Rev. 95 217 (1954).

[Bru56] Brueckner K., Phys. Rev. 103 1121 (1956).

[BSC64] Bunker M., Starner J. and Stephens F., Bull. Am. Phys. Soc. 9 18 (1964).

[Chi+90] Chiba S., Guenther P., Lawson R. and Smith A., Phys. Rev. C42 2487 (1990); and references cited therein.

[CL55] Cranberg L. and Levin J., Proc. Conf. on Peaceful Uses of Atomic Energy, Geneva (United Nations Press, New York, 1958).

[CSL83] Nuclear Standards File, IAEA Tech. Report 227, eds. Conde H., Smith A. and Lorenz A. (1983); also the ENDF/B-6 standards file.

[ENDF] Evaluated Nuclear Data File/B, version 6; available from the National Nuclear Data Center, Brookhaven National Laboratory. The particular file for ^{165}Ho is Mat. number 6725, prepared by Young P. and Arthur E. (1988).

[Fas+69] Fasoli U. et al, Nucl. Phys. A133 572 (1969); see also Nuovo Cemento Lett. 6 485 (1973).

[FCR77] Ferrer J., Carlson J. and Rapaport J., Nucl. Phys. A275 325 (1977).

[Fes58] Feshbach H., Ann. Rev. Nucl. Sci. 8 49 (1958).

[FH62] Fuller E. and Hayward E., Nucl. Phys. 30 613 (1962).

[FHM69] Fisher T., Healey D. and McCarthy J., Nucl. Phys. A130 609 (1969).

[GC65] Gilbert A. and Cameron A., Can. J. Phys. 43 1446 (1965).

[GPT68] Greenlees W., Pyle G. and Tang Y., Phys. Rev. 171 1115 (1968); see also Phys. Rev. C1 1145 (1970).

[GS58] Green A. and Sood P., Phys. Rev. 111 1147 (1958).
[GT63] Gilboy W. and Towle J., Nucl. Phys. 42 86 (1963)
[HF52] Hauser W. and Feshbach H., Phys. Rev. 87 362 (1952).
[Hod71] Hodgson P. E., Nuclear reactions and nuclear structure (Clarendon, Oxford, 1971).
[Hod94] Hodgson P. E., The nucleon optical model (World Scientific, Singapore, 1994).
[JLM77] Jeukenne J., Lejeune A. and Mahaux C., Phys. Rev. C16 80 (1977).
[Lan62] Lane A., Nucl. Phys. 55 676 (1962); also Phys. Rev. Lett. 8 171 (1962).
[LGS87] Lawson R., Guenther P. and Smith A., Phys. Rev. C36 1298 (1987).
[Lip66] Lipperheide R., Nucl. Phys. 89 97 (1966).
[MBA75] Madsen V., Brown V. and Anderson J., Phys. Rev. C12 1205 (1975).
[MDH81] Mughabghab S., Divadeenam M. and Holden N., Neutron cross sections (Academic, New York, 1981).
[Mea+71] Meadows J. et al., Z. Phys. 243 171 (1971).
[MN59] Mottelson B. and Nilsson S., Danske, K.: Vidensk. Selsk. mat-fysk., Skir. 1 No. 8 (1959).
[MN81] Mahaux C. and Ngo H., Phys. Lett. 100B 285 (1981).
[Mol80] Moldauer P. A., Nucl. Phys. A344 185 (1980).
[Mol82] Moldauer P. A., Spherical optical-statistical model code ABAREX, private communication (1982); extensively modified and document by Smith A. and Lawson R. in the Argonne National Laboratory Report ANL/NDM-148 (1998).
[MRT66] Marshak H., Richardson A. and Tamura T., Phys. Rev. 150 996 (1966).
[NDS] Pekar L., Nucl. Data Sheets 65 439 (1992); also Pekar L., Nucl. Data Sheets 50 137 (1986).
[NNDC] National Nuclear Data Center, Brookhaven National Laboratory.
[OE60] Olson M. and Elbeck B., Nucl. Phys. 15 134 (1960).
[Pas67] Passatore G., Nucl. Phys. A95 694 (1967).
[PB62] Perey F. and Buck B., Nucl. Phys. 32 353 (1962).
[PP76] Perey C. and Perey F., At. Data and Nucl. Data Tables, 17 1 (1976).
[Pre62] Preston M., Physics of the nucleus (Addison-Wesly, Reading, MA, 1962).
[Ray96] Raynal J., The coupled channels code ECIS96, private communication (1996); see also CEA Report, CEA-N-2772 (1994).
[Sat83] Satchler G., Direct nuclear reactions (Clarendon, Oxford, 1983).
[Smi80] Smith A., Argonne National Laboratory memorandum, unpublished (1980).
[Smi91] Smith A., Argonne National Laboratory memorandum, unpublished (1991).
[Smi+92] Smith A. et al., Argonne National Laboratory Report ANL/NDM-127 (1992); Phys. Rev. C45 (1992) 1260; Z. Phys. A306 (1982) 265; Nucl. Instr. Methods 50 (1977) 277; and references cited therein.
[Smi97] Smith A., J. Phys. G24 637 (1997).

[Smi97A] Smith A., Argonne National Laboratory Report ANL/NDM-147 (1997); and references cited therein.
[Tam65] Tamura T., Rev. Mod. Phys. 37 679 (1965).
[Tul90] Tuli J., Nuclear Wallet Cards, NNDC (1990).
[Wag+65] Wagner R. et al., Phys. Rev. B139 29 (1965).
[WG86] Walter R. and Guss P., Proc. Conf. on Nucl. Data for Basic and Applied Sci., eds. Young P. et al., vol.-2, p.-277 (Gordon and Breach, New York, 1986).
[Wol51] Wolfenstein L., Phys. Rev. 82 690 (1951).
[WWG60] Wyatt P., Wills J. and Green A., Phys. Rev. 119 1031 (1960).
[You86] Young P., Los Alamos National Laboratory Report LA-10689-PR (1986); also private communication (1999).
[YA88] Young P. and Arthur E., ENDF/B-6 documentation (1988)

B. Total cross sections

[Fas+69] Fasoli U. et al., Nucl. Phys. A133 572 (1969).
(EXFOR 20976)
[Fas+73] Fasoli U. et al., Nuovo Cemento Lett. 6 485 (1973).
(EXFOR 20497)
[Fis+67] Fisher T. et al., Phys. Rev. 157 1149 (1967).
(EXFOR 12118)
[FG71] Foster D. and Glasgow D., Phys. Rev. C3 576 (1971).
(EXFOR 10047)
[GT63] Gilboy W. and Towle J., Nucl. Phys. 42 86 (1963).
(EXFOR 21110)
[Gio+78] Giordano V. et al., Nucl. Phys. A302 83 (1978).
(EXFOR 20806)
[Kel+74] Kellie J. et al., J. Phys. A7 1758 (1974).
(EXFOR 20148)
[Kob+61] Kobayashi S. et al., J. Phys. (Japan) 22 368 (1961).
(EXFOR 20293)
[MRT66] Marshak H., Richardson A. and Tamura T., Phys. Rev. 150 996 (1966).
(EXFOR 12142)
[Mar+70] Marshak H. et al., Phys. Rev. C2 1862 (1970).
(EXFOR 10076)
[McC+68] Mc Carthy J. et al., Phys. Rev. Lett. 20 502 (1968).
(EXFOR 12122)
[Mea+71] Meadows J. et al., Z. Phys. 243 171 (1971).
(EXFOR 10034)
[SMS66] Stupegia D., Madsen A. and Schmidt M., private communication.
(EXFOR 12125)
[Wag+65] Wagner R. et al., Phys. Rev. B139 29 (1965).
(EXFOR 12133)

C. Differential scattering cross sections

[Fas+69] Fasoli U. et al., Nucl. Phys. A133 572 (1969).
(EXFOR 20976)

[FCR77] Ferrer J., Carlson J. and Rapaport J., Nucl. Phys. A275 325 (1977).
(EXFOR 10633)
[GT63] Gilboy W. and Towle J., Nucl. Phys. 42 86 (1963).
(EXFOR 21110)
[Gio+78] Giordno V. et al., Nucl. Phys. A302 83 (1978).
(EXFOR 20806)
[Mea+71] Meadows J. et al., Z. Phys. 243 171 (1971).
(EXFOR 10034)
[Wag+65] Wagner R. et al., Phys, Rev. B139 29 (1965).
(EXFOR 12133)

Table 3-2-1. SOM model parameters, energies in MeV, dimensions, in fermis, strengths in volume-integrals-nucleon (J_i) in MeV-Fm^3, and potential depths in MeV.

Real potential

Depth V = 45.467 - 0.045·E
Strength J_v = 349.6 - 0.349·E
r_v = 1.199
a_v = 0.553

Imaginary potential

Depth W = 6.214 - 0.161·E
Strength J_w = 77.76 - 2.016·E
r_w = 1.266
a_w = 0.815

Spin-orbit potential [WG86]

Depth V_{so} = 6.143 - 0.015·E
r_{so} = 1.103
a_{so} = 0.560

Table 3-3-1. CCM model parameters, energies in MeV, dimensions, in fermis, strengths in volume-integrals-nucleon (J_i) in MeV-Fm^3, and potential depths in MeV.

Real potential

Depth $V = 46.211 - 0.370 \cdot E$
Strength $J_v = 444.4 - 3.558 \cdot E$
$r_v = 1.260$
$a_v = 0.630$

Imaginary potential

Depth $W = 3.134 + 0.301 \cdot E$
Strength $J_w = 22.40 + 2.151 \cdot E$
$r_w = 1.260$
$a_w = 0.480$

Spin-orbit potential [You86]

Depth $V_{so} = 6.0$
$r_{so} = 1.26$
$a_{so} = 0.63$

Deformations

$\beta_2 = 0.30$
$\beta_4 = -0.02$

Table 3-4-1. CCMD model parameters, energies in MeV, dimensions, in fermis, strengths in volume-integrals-nucleon (J_i) in MeV-Fm^3, and potential depths in MeV.

Real potential

Depth V = 46.525 - 0.506·E
Strength J_v = 426.4 - 4.638·E
r_v = 1.239
a_v = 0.630

Imaginary potential

Depth W = 3.920 + 0.197·E
Strength J_w = 28.10 + 1.412·E
r_w = 1.260
a_w = 0.480

Spin-orbit potential [You86]

Depth V_{so} = 6.0
r_{so} = 1.26
a_{so} = 0.63

Deformations

β_2 = 0.30
β_4 = -0.02

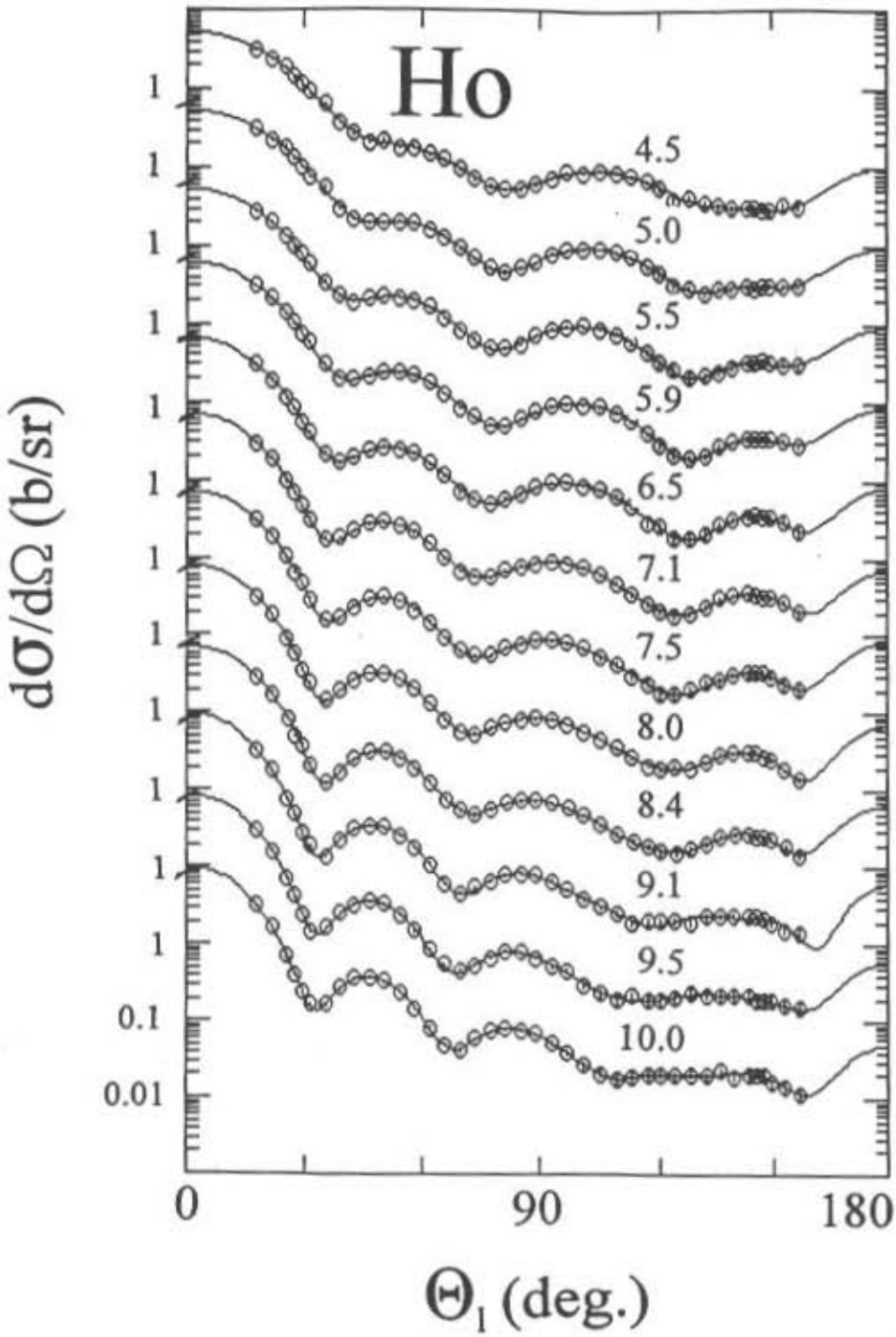


Fig. 2-1. Measured differential elastic-scattering cross sections of holmium. The present results are indicated by circular data symbols. Curves denote the results of fitting legendre-polynomial expansions to the measured values. Approximate incident energies are numerically noted in MeV. Herein, all data is presented in the laboratory coordinate system.

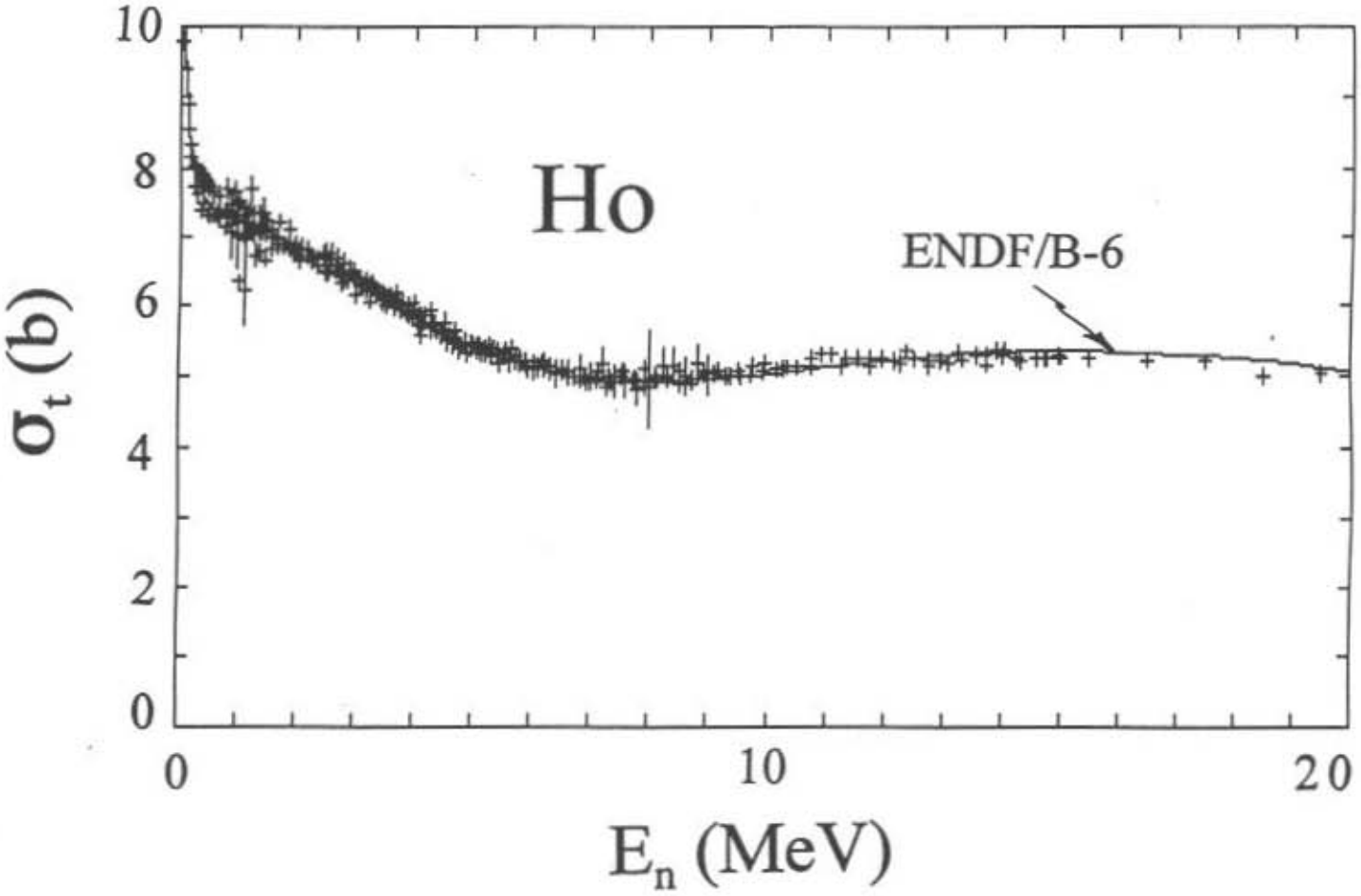


Fig. 3-1-1. Comparison of the energy-averaged experimental neutron total-cross sections (+ symbols) with the corresponding ENDF/B-6 values (curve).

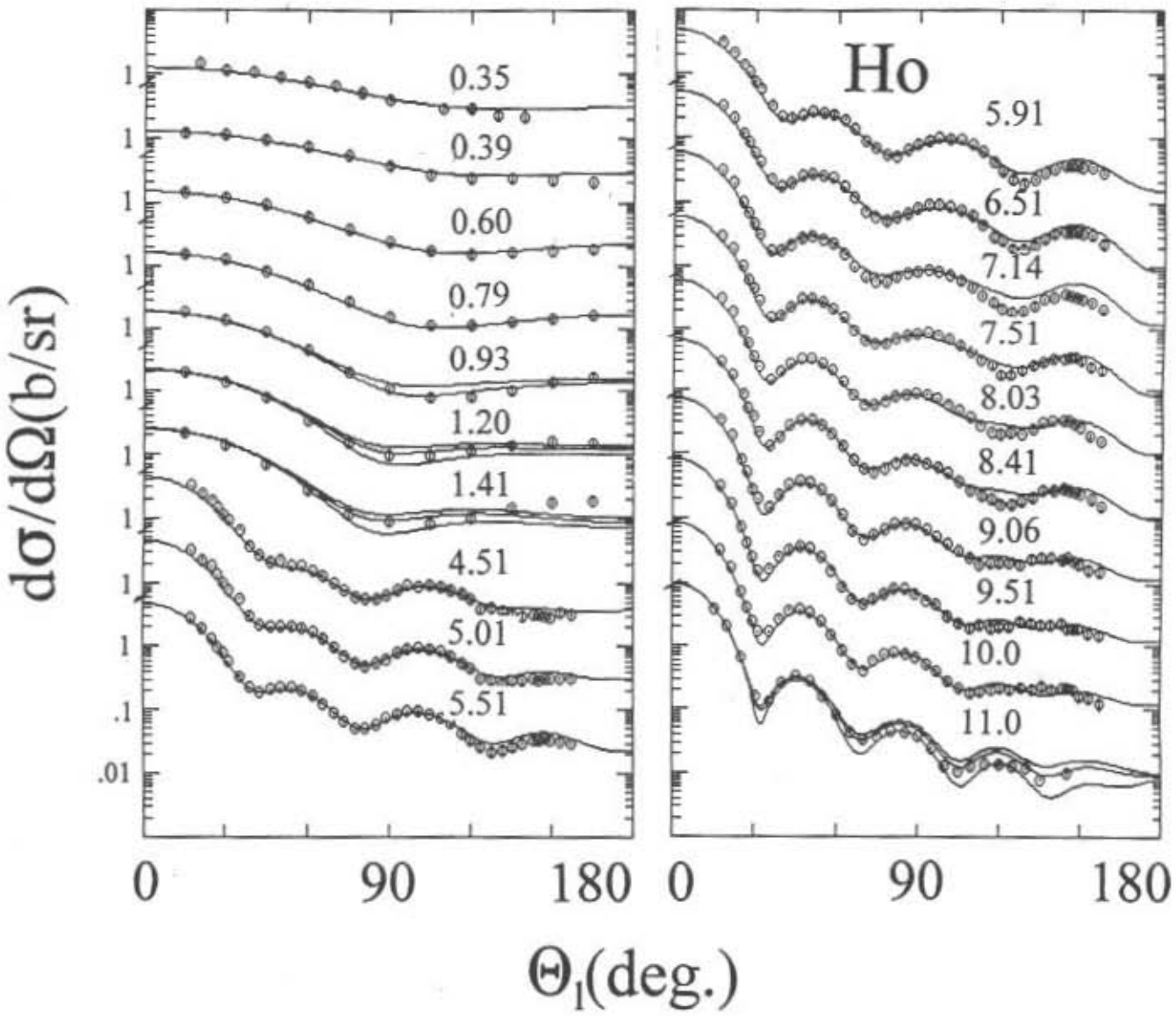


Fig. 3-1-2. Comparison of the differential-scattering data base (data symbols) with the results of CCM calculations (curves). Approximate incident energies are numerically noted in MeV. Where there are two or more curves at a single incident energy they represent different resolution assumptions as defined in the text.

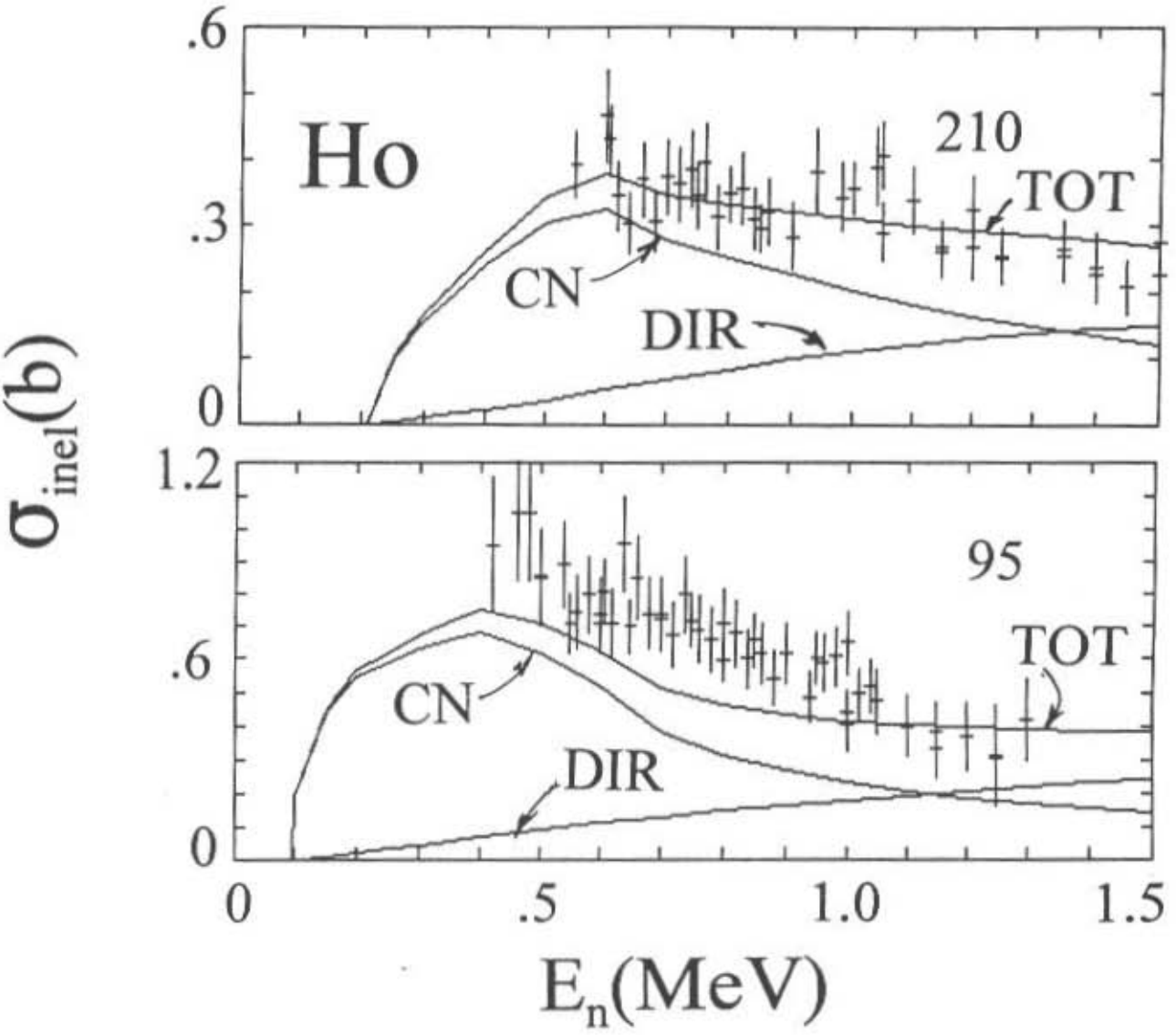


Fig. 3-1-3. Comparison of measured and calculated neutron inelastic-scattering excitation cross sections of the first two excited levels of the $K = 7/2^-$ ground-state rotational band of ^{165}Ho. "+" symbols denote the experimental results of ref. [Mea+71]. Approximate excitation energies (95 and 210 keV) are numerically noted in the respective panels of the figure. Curves denote the results of calculations using the CCM model where "CN" is the compound-nucleus component, "DIR" the direct-reaction contribution and "TOT" the sum of the CN and DIR contributions.

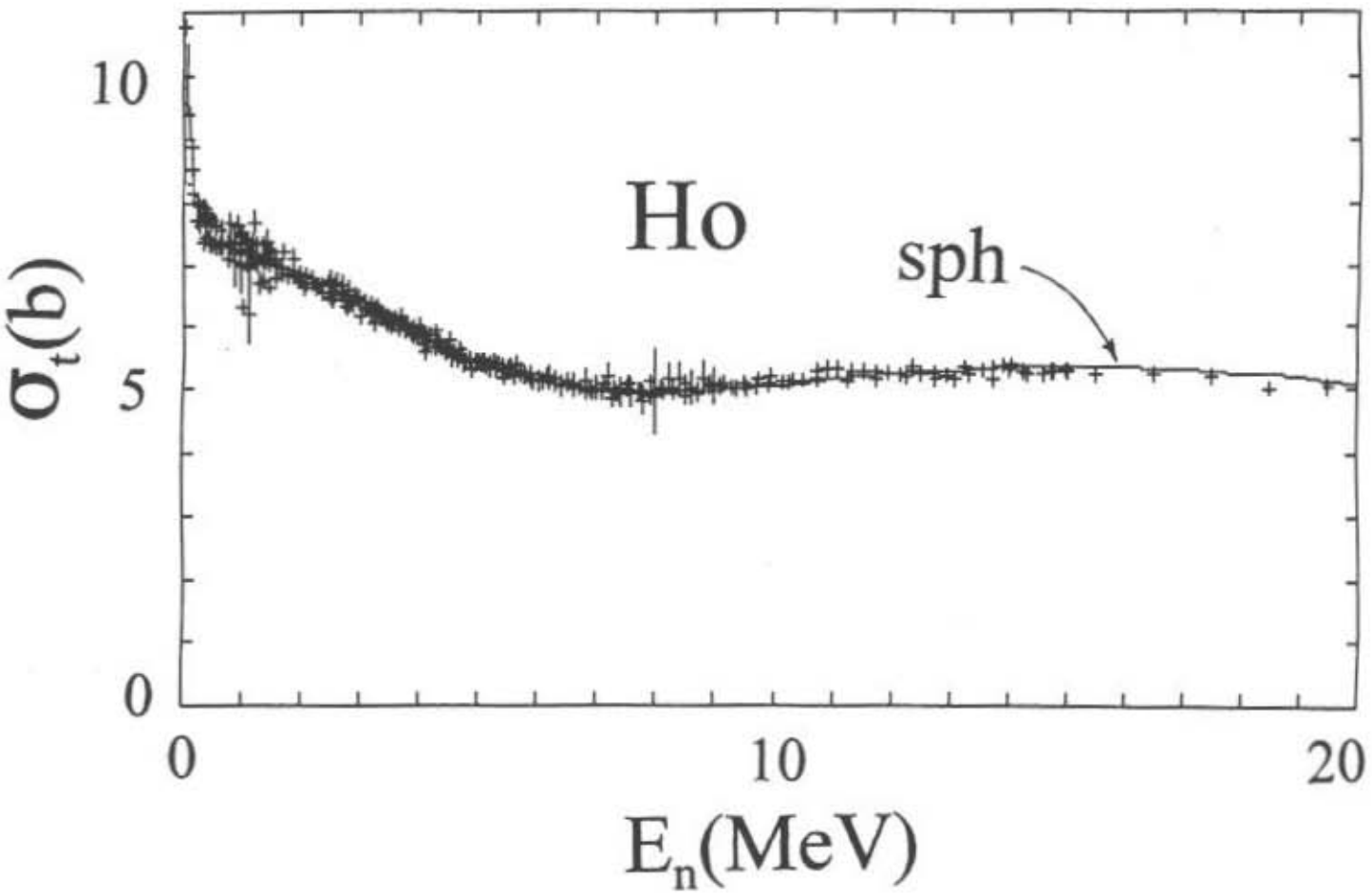


Fig. 3-2-1. Comparison of measured and calculated ^{165}Ho neutron total cross sections. Energy-averaged experimental values are indicated by "+" symbols and the "sph" curve denotes the results of SOM calculations.

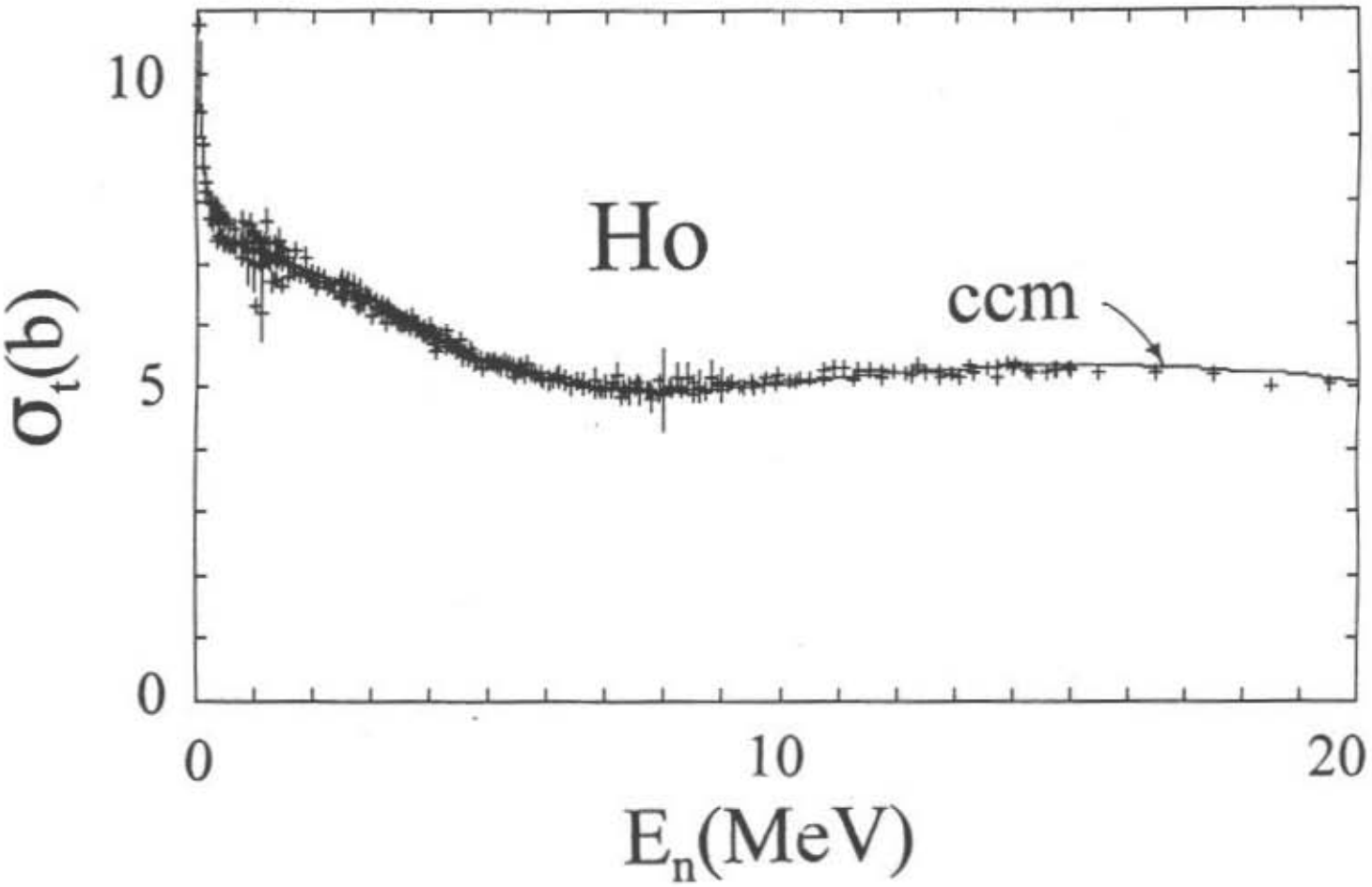


Fig. 3-3-1. Comparison of measured (symbols) and calculated (curve) neutron total cross section of ^{165}Ho. The calculations used the CCM model as noted on the figure.

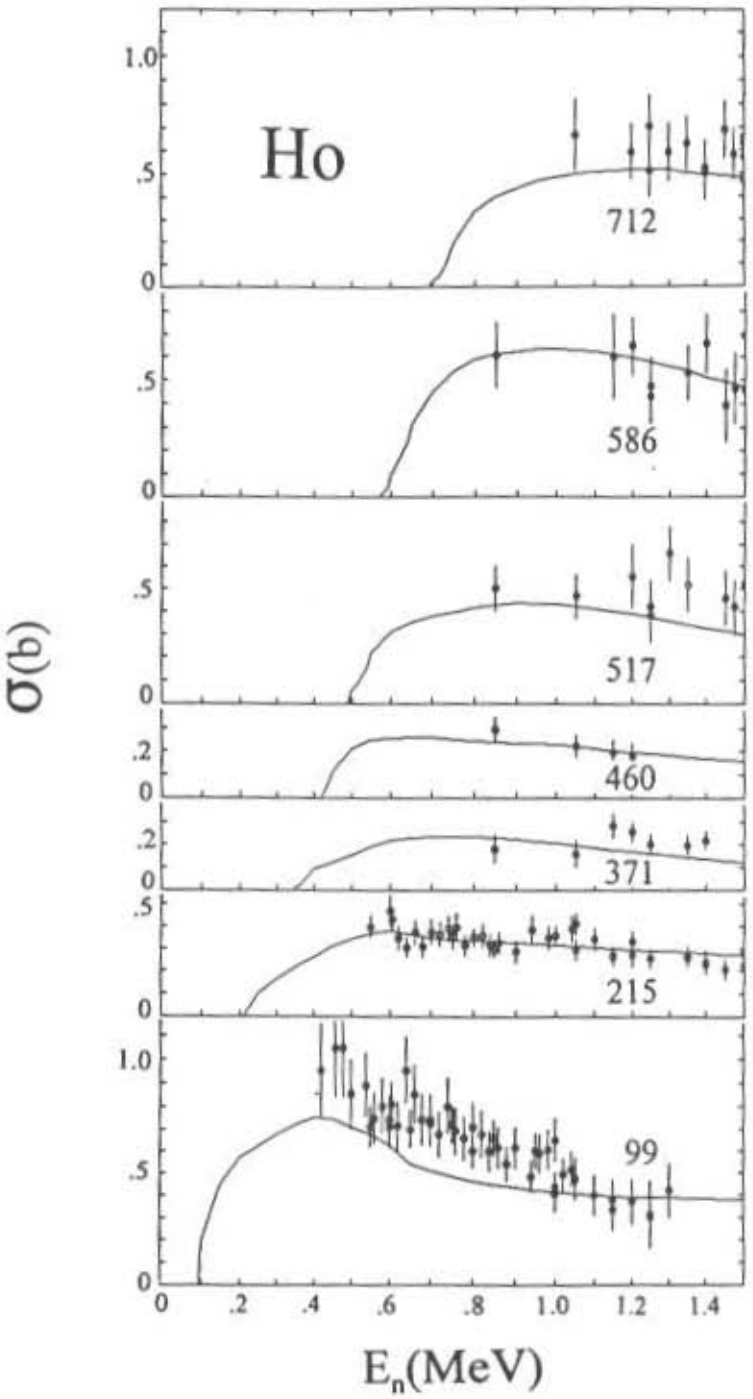


Fig. 3-3-2. Comparison of measured and calculated inelastic excitation cross sections of ^{165}Ho. The experimental values, taken from ref. [Mea+71], are indicated by "o" symbols. Curves indicate the results of CCM calculations. Numerical values in each panel of the figure indicate the mean excitation energies reported from the measurements [Mea+71].

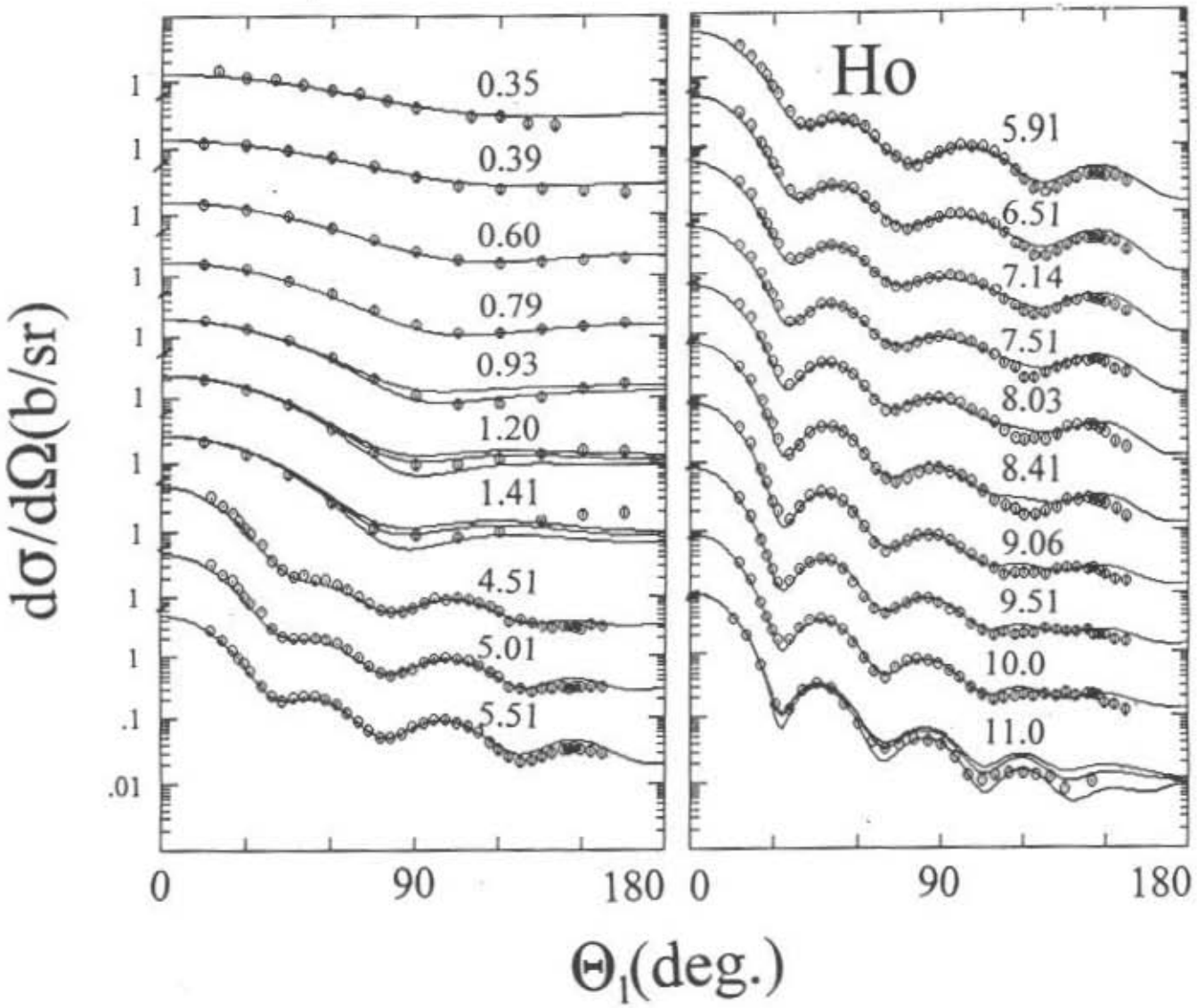


Fig. 3-4-1. Comparison of the differential-scattering data base (symbols) with the results of CCMD calculations (curves). The notation is identical to that of Fig. 3-1-2.

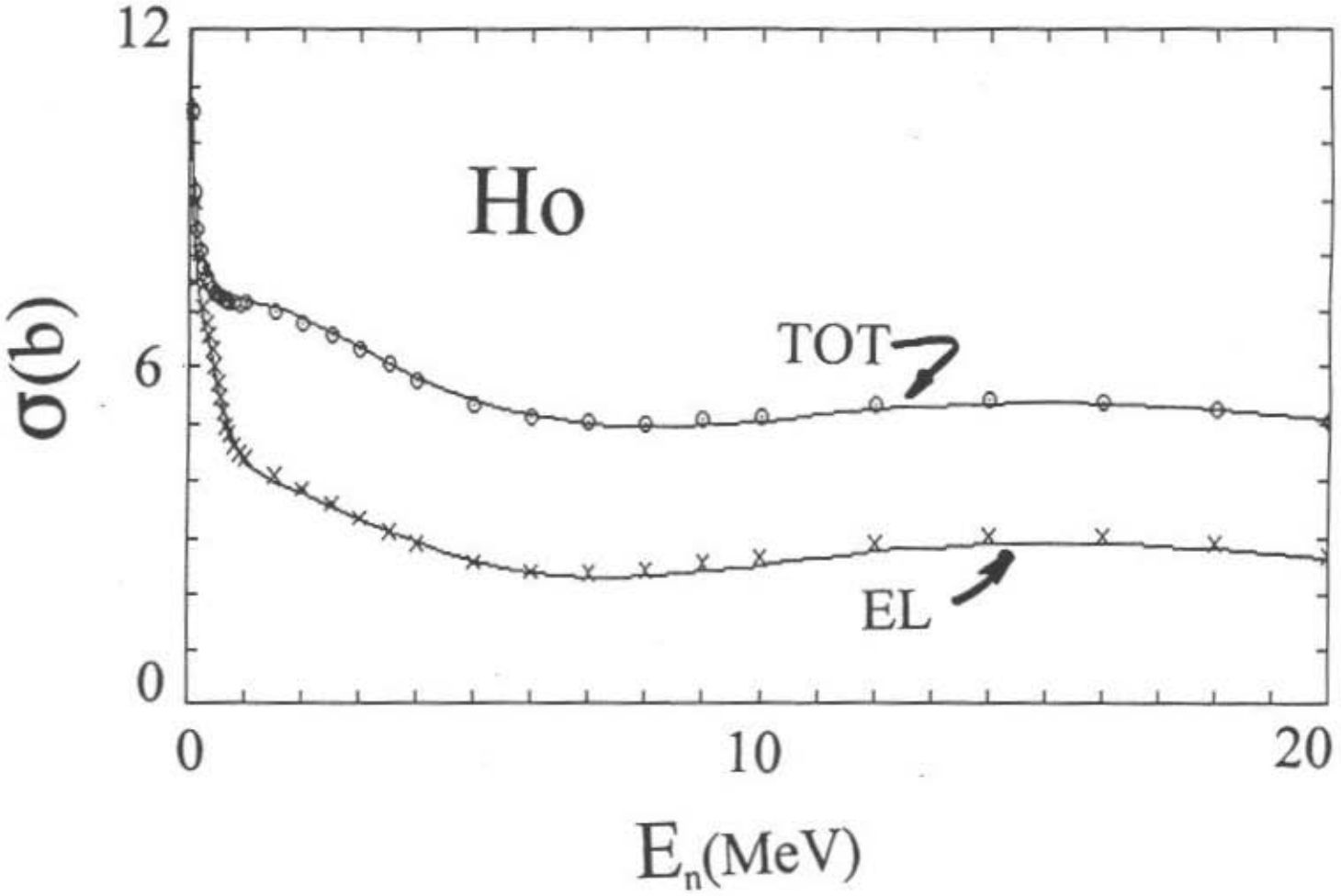


Fig. 4-1. Comparison of ENDF/B-6 [YA88] neutron total and elastic-scattering cross sections with the predictions of the present CCM model. Simple curves indicate the ENDF/B-6 results and symbols the results of CCM calculations.

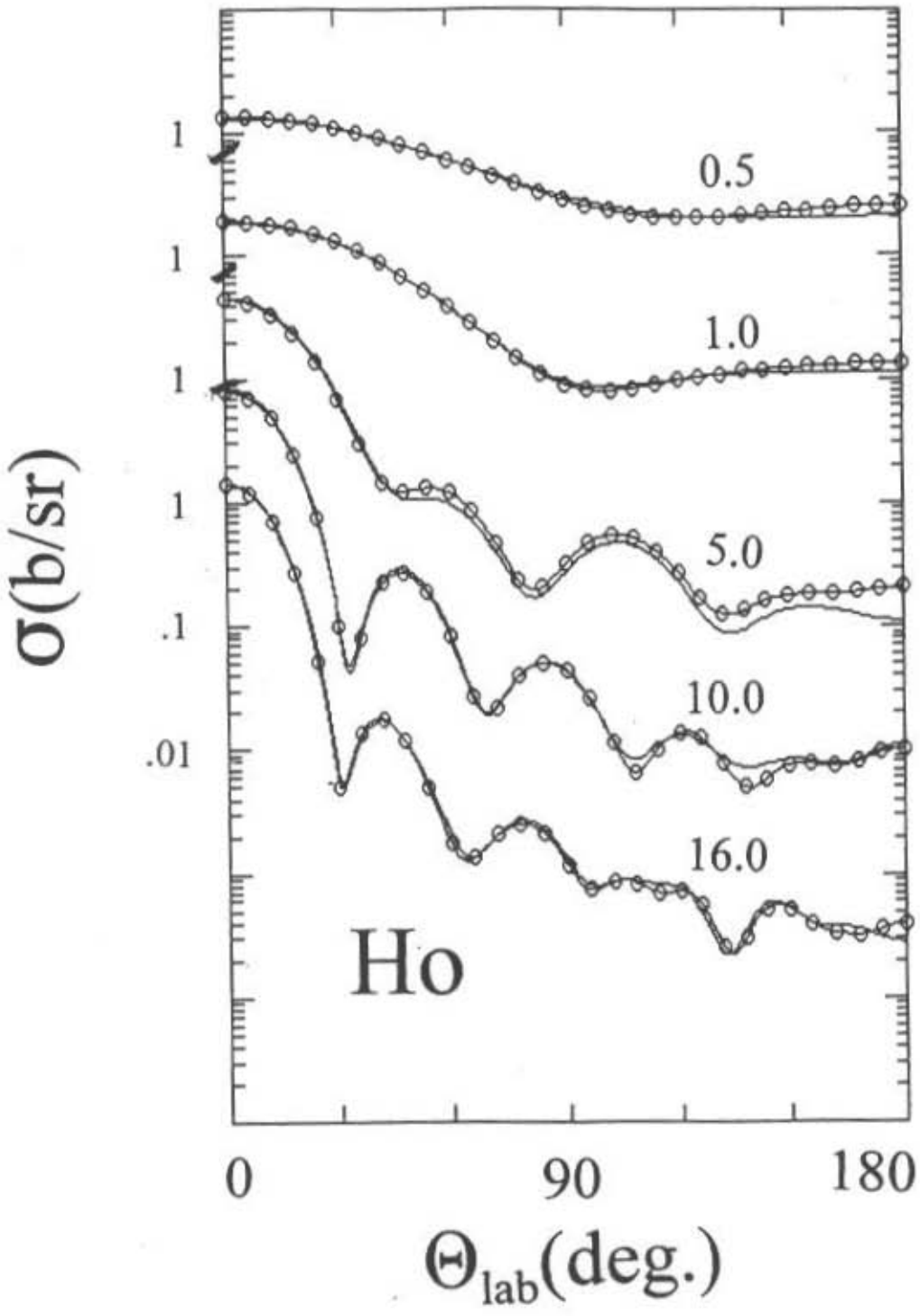


Fig. 4-2. Comparisons of ENDF/B-6 [YA88] and the present CCM differential elastic scattering. The simple curves indicate ENDF/B-6 results and curves with circular symbols the results obtained with the present CCM model. Incident neutron energies are numerically noted.

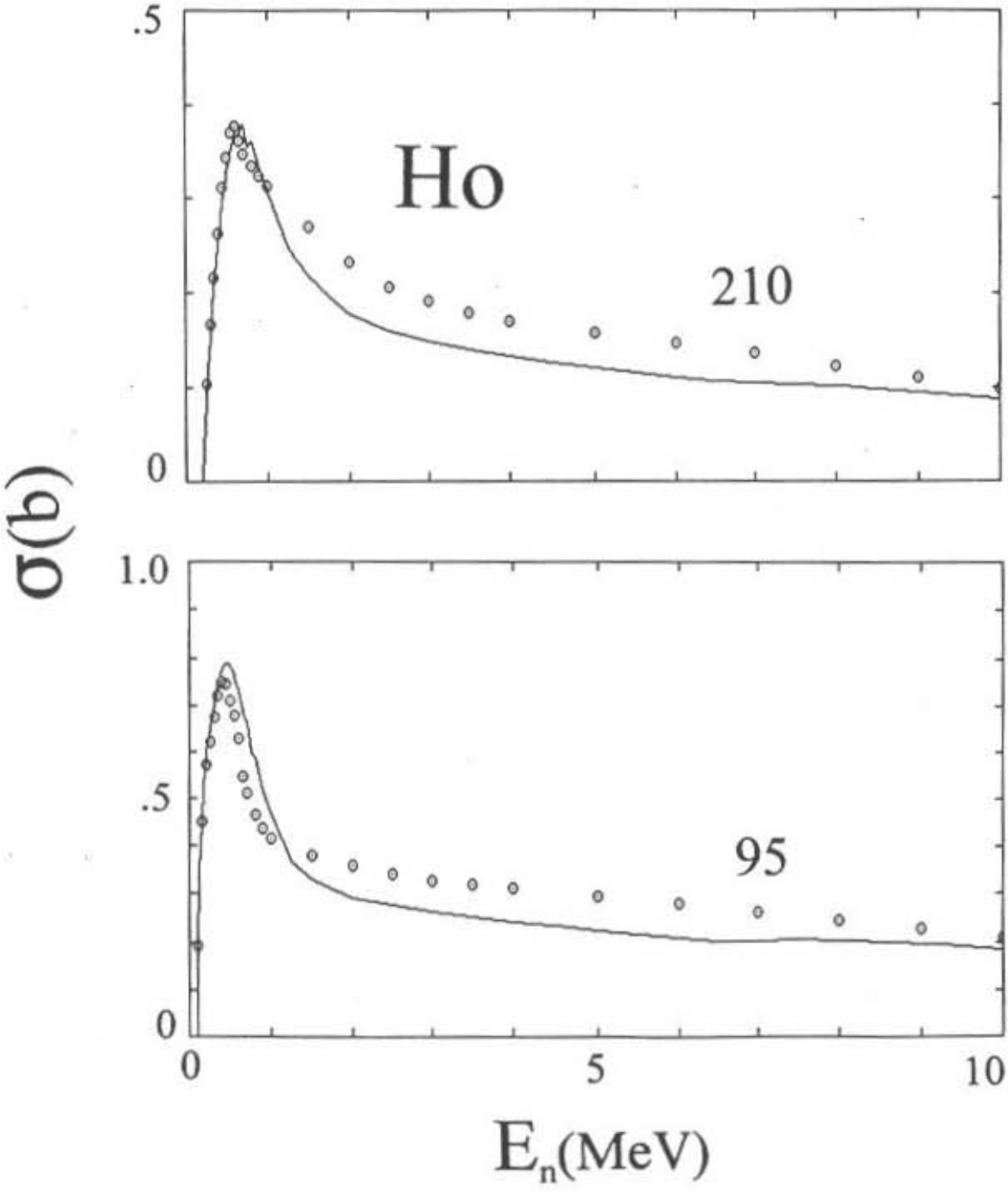


Fig. 4-3. Comparisons of the ENDF/B-6 (simple curves) and CCM-calculated results (symbols) for the neutron excitation of the first two excited members of the $K = 7/2^-$ ground-state rotational band of ^{165}Ho. Approximate excitation energies are numerically noted in keV.